Charge disproportionation in $La_{1-x}Sr_xFeO_3$ probed by diffraction and spectroscopic experiments

Javier Blasco,* Bartolomé Aznar, Joaquín García, Gloria Subías, Javier Herrero-Martín, and Jolanta Stankiewicz
Instituto de Ciencia de Materiales de Aragón and Departamento de Física de la Materia Condensada, CSIC-Universidad de Zaragoza, Pedro Cerbuna 12, 50009 Zaragoza, Spain
(Received 6 July 2007; published 25 February 2008)

The crystal and local structures of $La_{1-x}Sr_xFeO_{3-\delta}$ $(0 \leqslant x \leqslant 1)$ samples have been studied by x-ray diffraction and x-ray absorption spectroscopy techniques. The Fe-O bond length decreases with increasing x. Accordingly, the x-ray absorption near edge spectroscopy (XANES) spectra reveal a chemical shift of the iron K edge to higher energies. Both results agree with an Fe valence increase as La is substituted with Sr. Extended x-ray absorption fine structure spectroscopy and XANES show that the chemical state of Fe atoms in intermediate compositions can be described either by a bimodal distribution of formal Fe^{3+} and Fe^{4+} ions or by an $Fe^{3.x+}$ intermediate valence. The large value of the Debye-Waller factors obtained for intermediate compositions indicates that hole doping produces local disorder around the Fe ions. These factors show unusually large values below the metal-insulator (MI) transition for $x=2/3$ or $3/4$. We show that a significant charge disproportionation of the type $2Fe^{4+} \rightarrow Fe^{3+}+Fe^{5+}$ cannot account for the local structure observed below the MI transition temperature of these samples. We suggest that an electronic localization arises from an order-disorder transition between dynamic and static distortions, resulting in the opening of a gap at the Fermi level.

DOI: 10.1103/PhysRevB.77.054107 PACS number(s): 61.05.cp, 61.66.Fn, 75.50.Ee, 72.15.Eb

I. INTRODUCTION

The perovskite series $La_{1-x}Sr_xFeO_3$ $(0 \leqslant x \leqslant 1)$ shows interesting changes in their physical properties as a function of composition.[1,2] $LaFeO_3$ is an antiferromagnetic insulator with a high Néel temperature (T_N) of approximately 750 K.[3] The substitution of La^{3+} with Sr^{2+} produces a formal change in the valence state of Fe ion from +3 $(x=0)$ to +4 $(x=1)$. This leads to the decrease of T_N and the increase of electronic conductivity.[4] The end member, $SrFeO_3$, is found to be a helical antiferromagnetic metal whose T_N is 134 K.[5]

One of the most striking properties in this series occurs at a critical concentration of $x \sim 2/3$. $La_{1/3}Sr_{2/3}FeO_3$ samples undergoes a metal-insulator (MI) transition at ~200 K, evidenced by a jump in the resistivity of more than 1 order of magnitude with decreasing temperature. This MI transition is accompanied by an antiferromagnetic ordering. A pioneering work on $La_{1-x}Sr_xFeO_3$, reporting Mössbauer spectroscopy results at low temperature, has revealed two kinds of Fe ions with different hyperfine fields,[6] which have been attributed to different charge states. In view of these results, the MI transition has then been interpreted as a charge disproportionation from an average-valence state $(Fe^{+3.67})$ in the paramagnetic phase above 200 K into a mixture of $2Fe^{3+}$ and $1Fe^{5+}$ in the antiferromagnetic charge ordering (CO) state below 200 K.[7] The Fe^{5+} comes from the disproportionation of Fe^{4+} into Fe^{3+} and Fe^{5+}. However, this transition is not accompanied by any significant lattice distortion although neutron diffraction experiments have revealed a spin-density wave along the [111] direction in the pseudocubic cell with two nonequivalent spin states for Fe ions.[8] Electron diffraction measurements have shown extra spots in the low-temperature phase,[9] and, recently, superlattice reflections due to charge and spin ordering have been observed by neutron diffraction measurements.[10,11] Nevertheless, there is no structural model that accounts for the low-temperature phase of $La_{1/3}Sr_{2/3}FeO_3$. In addition, the magnetic moments found for the two nonequivalent Fe ions seem to depend on the synthetic route.[8,11] Finally, the occurrence of this type of CO transitions also depends on the rare-earth size.[12,13]

A detailed crystal characterization for the whole series of $La_{1-x}Sr_xFeO_3$ was reported, and changes associated with the substitution of Sr for La have been studied.[14] $LaFeO_3$ exhibits the orthorhombic distortion of a perovskite with space group $Pbnm$, while intermediate compounds show a rhombohedral cell $(R\text{-}3c)$, and $SrFeO_3$ is cubic with space group $Pm\text{-}3m$.[14] Accordingly, the iron coordination geometry becomes more regular by increasing the Sr content.

The hole doping in $LaFeO_3$ gives rise to structural and magnetic transitions based on the change in electronic configuration of the Fe and/or O sites. However, only few studies have been reported on the electronic structure of the series.[15–18] Soft x-ray absorption and electron spectroscopies have revealed that holes created by Sr doping have a mixed Fe $3d-$O $2p$ character for high Sr content whereas they are mainly of the O $2p$ character for low Sr content.[15] Combined studies with photoemission spectroscopy have confirmed this point and suggested that the hole ordering on the oxygen sites plays an essential role in realizing the charge disproportionated state.[16]

The present work was undertaken with the aim of gaining insight into the changes of the electronic and local structure of Fe atoms upon varying the La/Sr ratio. It also focuses on the changes observed at the so-called CO transition at the critical concentrations of $x=2/3$ and $x=3/4$. The information about either the Fe oxidation state or the local structure is directly obtained by x-ray absorption spectroscopy (XAS) at the Fe K edge. Previously reported x-ray absorption near edge spectroscopy (XANES) results at the Fe K edge were used to characterize the valence of Fe along the series of $La_{1-x}Sr_xFeO_3$.[17] The authors found an increase of the valence of Fe with increasing Sr/La ratio, which saturates at $x=0.8$. Extended x-ray absorption fine structure spectroscopy (EXAFS) was only studied on selected samples $(x=0.2)$, which

TABLE I. Selected structural parameters (space group, lattice constants, and volume/f.u.), oxygen content, and average Fe–O bond length for $La_{1-x}Sr_xFeO_{3\pm\delta}$. The x value is given for each column, and Z values are 4, 6, and 1 for *Pbnm*, *R*-3*c*, and *Pm*-3*m*, respectively. Numbers in parentheses refer to the standard deviation of the last significant digit.

Sample (x)	0	1/8	1/4	1/3	1/2	2/3	3/4	7/8	1
Space group	*Pbnm*	*Pbnm*	*Pbnm*	*R*-3*c*	*R*-3*c*	*R*-3*c*	*Pm*-3*m*	*Pm*-3*m*	*Pm*-3*m*
a (Å)	5.5568(4)	5.5464(4)	5.5508(5)	5.5350(1)	5.5072(1)	5.4787(2)	3.8664(1)	3.8580(1)	3.8530(1)
b (Å)	5.5656(4)	5.5491(2)	5.5167(3)						
c (Å)	7.8496(7)	7.8356(8)	7.8151(9)	13.4309(4)	13.4119(4)	13.4080(6)			
Vol/Z (Å^3)	60.69(1)	60.29(1)	59.83(1)	59.39(1)	58.71(1)	58.09(1)	57.801(2)	57.424(2)	57.201(3)
$3\pm\delta$	3.004(10)	3.041(11)	3.025(12)	3.028(10)	3.011(9)	3.013(12)	2.980(8)	2.984(9)	2.961(11)
⟨Fe-O⟩ (Å)	2.006	1.987	1.970	1.965	1.951	1.939	1.9332	1.929	1.9265
Fe^{4+} (%)	0.8	20.7	30	36.6	52.2	69.6	71	84.3	92.2

are promising cathode materials.[18] In particular, we have not found any complete XAS study of samples showing the CO transition. This is surprising since XAS studies are very useful in characterizing order-disorder transitions[19] and in evaluating oxidation states in mixed oxides.[20]

II. EXPERIMENTAL METHODS

$La_{1-x}Sr_xFeO_{3-\delta}$ $(x=0,1/8,1/4,1/3,1/2,2/3,3/4,7/8,1)$ samples were prepared[13] using solid-state methods. Stoichiometric amounts of La_2O_3, $SrCO_3$, and Fe_2O_3 were mixed, ground, and calcined at 1000 °C for 1 d in air. Then, the powders were ground, pressed into pellets and sintered at 1250 °C for 1 d, also in air. The last step was repeated one more time with a final annealing at 450 °C for 10 h in the same atmosphere. Samples with $x>0.5$ were tempered at 450 °C for 1 d at high oxygen pressure (200 bars) in a Morris Research furnace in order to improve the oxygen stoichiometry.

The samples were characterized by x-ray powder diffraction (XRD) using a Rigaku D-Max system. Step-scanned patterns were measured between 10° and 120° (in steps of 0.03°) at room temperature. The x-ray system was working at 40 kV and 80 mA with a counting rate of 4 s step^{-1}. We used a graphite monochromator to select the Cu $K\alpha$ radiation. The crystal structures were refined by the Rietveld method using the FULLPROF package program.[21]

To obtain the oxygen content, we used the method of redox titration with cerium (IV) sulfate and Mohr's salt.[22,23] Powdered samples (~100 mg) were dissolved with an excess of Mohr's salt in 3*M* HCl. At this step, tetravalent Fe is reduced into Fe^{3+} by divalent irons. After heating for a few minutes, yellow solutions are obtained. 10 ml of concentrated phosphoric acid is then added to form a colorless complex of Fe^{3+}. After cooling, the excess of Fe^{2+} ions is titrated with a $Ce(SO_4)_2$ solution using ferroin (one drop) as an indicator. The whole titration process is carried out under an Ar stream. The end point is detected as a sudden change from red-orange to colorless (or very light blue) solution. This analysis was repeated three times for each sample and the standard deviation in δ is estimated to be ± 0.01.

The a/c magnetic susceptibility was measured between 5 and 300 K in a commercial Quantum Design superconducting quantum interference device magnetometer. Resistivity measurements were carried out using the standard six-probe ac method in the temperature range between 4 and 300 K. We checked the type of carriers using the hot probe.

XAS spectra were recorded at the BM29 beamline of the ESRF in Grenoble (France).[24] The storage ring was operating at 6 GeV electron energy and ~200 mA electron current. The measurements were carried out in transmission mode on powder samples and at selected temperatures between 40 and 295 K. The beam was monochromatized by a fixed-exit Si(111) double crystal, and harmonic rejection better than 10^{-5} was achieved by using the Si mirror coating of the double flat mirror installed after the monochromator. The energy resolution $\delta E/E$ was estimated to be about 8×10^{-5} at the Fe *K* edge, and an Fe foil was simultaneously measured for energy calibration. The XANES spectra were normalized to the high energy part of each spectrum (~100 eV beyond the edge) after background subtraction. We have also recorded XANES spectra of Fe, FeO, Fe_3O_4, and Fe_2O_3 as references for the Fe *K* edge.

The EXAFS structural analysis was performed using the ARTEMIS program,[25] which makes use of theoretical standards calculated from FEFF6.[26] This software was also used to perform the background removal. The fits were carried out in the *R* space using a sine window and clusters of ~4 Å, which include contributions from the first, second, and third shells. However, we limit our discussion to the first coordination shell because it is correlated to the main physical properties.

III. RESULTS

The whole $La_{1-x}Sr_xFeO_{3-\delta}$ series was characterized at room temperature by means of XRD. All the studied samples showed single phase, and selected refined parameters are summarized in Table I. Overall, our diffraction results concur with previous reports.[14] Samples with low Sr content ($x<1/3$) crystallize in a distorted perovskite structure with an orthorhombic *Pbnm* space group. A rhombohedral cell, *R*-3*c*, is found for intermediate compositions $(1/3\leqslant x\leqslant 2/3)$, whereas Sr-rich samples are cubic $(x\geqslant 3/4)$.

Although the 12-fold coordinated Sr^{2+} cation[27] is bigger than La^{3+}, the volume/f.u. decreases continuously as the con-

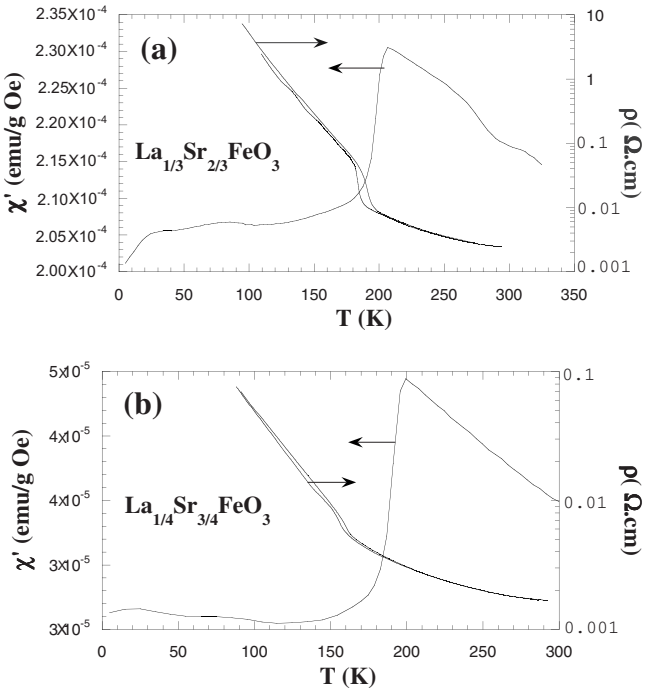

FIG. 1. Resistivity and ac magnetic susceptibility vs temperature for (a) $La_{1/3}Sr_{2/3}FeO_3$ and (b) $La_{1/4}Sr_{3/4}FeO_3$.

tent of Sr is increased. This indicates that the unit cell volume mainly depends on the oxidation state of Fe atoms, which continuously increases with increasing content of Sr. It also leads to a decrease of the average Fe-O distances as the Sr/La ratio increases. A chemical analysis confirms the oxidation of Fe with increasing doping ratio. It also reveals that our synthetic routes led to samples with a slight oxygen excess for La-rich compounds, while the Sr-rich ones show a small oxygen deficiency in spite of the annealing at high oxygen pressure.

Resistivity measurements revealed a semiconducting behavior for all samples, even for $SrFeO_{2.96}$. The resistivity found for the latter may be attributed to the presence of oxygen vacancies.[13] The activation energy strongly decreases with increasing doping ratio; it amounts to 5 meV for $SrFeO_{2.96}$. We have also found two samples exhibiting clear conductivity transitions, namely, $x=2/3$ and $x=3/4$. Their resistivity variation with temperature is displayed in Fig. 1. $La_{1/3}Sr_{2/3}FeO_3$ shows a semiconducting behavior at room temperature with a sudden increase (~1 order of magnitude) at the CO transition between 180 and 200 K. This transition shows thermal hysteresis, suggesting a first order transition. The low-temperature phase is highly resistive with large activation energy. The other sample, $La_{1/4}Sr_{3/4}FeO_3$, shows a similar transition at lower temperatures. Here, the resistivity jump is much smaller.

We also measured ac magnetic susceptibility for samples with $x \geqslant 0.5$. Anomalies related to antiferromagnetic ordering are clearly seen for these samples. T_N decreases from ~225 K ($x=0.5$) down to ~130 K ($x=1$). The susceptibility curves for $x=2/3$ and $\frac{3}{4}$ are also plotted in Fig. 1. It is clear that magnetic and MI transitions are coupled for $x=2/3$ but not for $x=3/4$.

A. Fe *K*-edge x-ray absorption near edge spectroscopy of $La_{1-x}Sr_xFeO_{3-\delta}$

Figure 2 shows the Fe *K*-edge XANES spectra of the

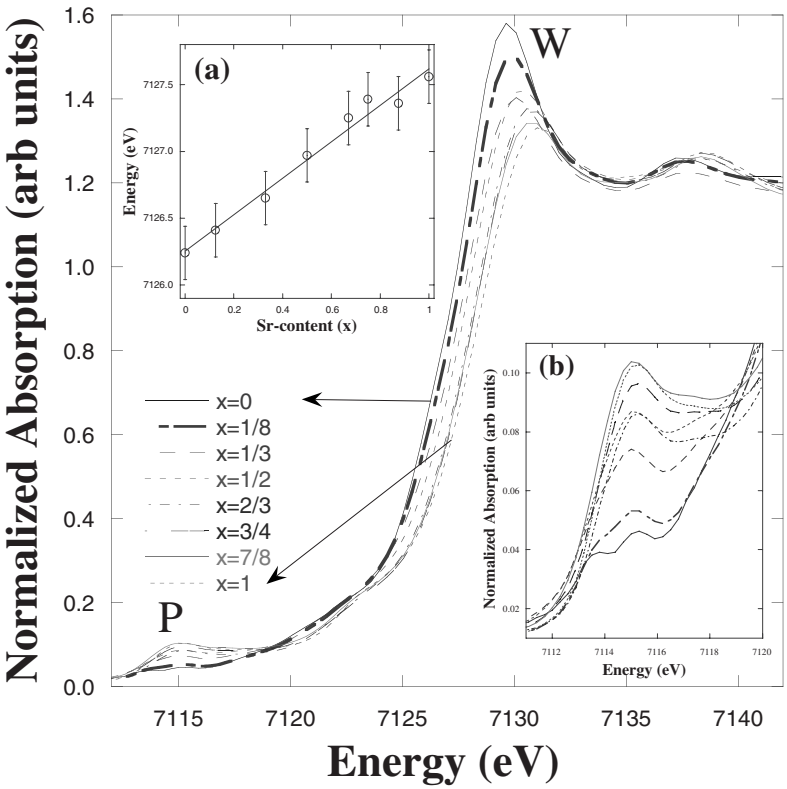

FIG. 2. XANES spectra at the Fe *K* edge for $La_{1-x}Sr_xFeO_3$ samples at room temperature. P and W denote prepeak and white line features, respectively. Inset (a): plot of the edge position vs chemical composition. The line is a linear fit of the experimental data. Inset (b): detail of the pre-edge region.

whole series at room temperature. This edge mainly probes the $1s \rightarrow np$ dipolar transitions. All spectra are alike. The main features of the spectra are a white line (denoted as W in the figure), whose intensity decreases as the Sr content increases, and prepeak features (P) at ~11 eV below the main edge.

We observe a systematic chemical shift of the edge position as the Sr content increases, indicating that the Fe valence also increases. Here, the edge was taken at the maximum of the first derivative of the XAS spectra, and the chemical shift between $LaFeO_3$ (formal Fe^{3+}) and $SrFeO_{2.96}$ (formal Fe^{4+}) was found to be 1.26 ± 0.2 eV, as can be seen in Fig. 2(a). The absorption edge for the doped samples lies between the end members, indicating intermediate valence states for iron. These results agree with the data reported earlier for the same series.[18] However, we obtain a slightly higher chemical shift, and we do not observe Fe valence saturation for $x \geqslant 3/4$. This can be related to the oxygen stoichiometry of the compounds. It seems that our samples are better oxidized because of the annealing at high oxygen pressure.

The pre-edge structures are usually attributed to quadrupole transitions from the $1s$ core state to $3d$ empty states, which are expected to be very weak for an iron atom in an octahedral environment. In addition, a significant contribution from dipole transitions can be expected in these compounds due to hybridization of the metal $3d$ states with the oxygen p band.[28] In this way, we observe prepeak changes along this series as can be seen in Fig. 2(b). The shape of these peaks changes, but the most important effect is an increase of its intensity as the content of Sr increases. In these oxides, the Fe atom is surrounded by six oxygen atoms forming an octahedron, and neighboring octahedra strongly interact with each other producing extended energy bands of mixed Fe $3d$ and O $2p$ character.[28] Thus, the increase in the intensity of these prepeaks can be related to an increase of the mixing between Fe $3d$ and O $2p$ states as the Fe valence (i.e., the hole count) increases, in agreement with the finding that samples with higher content of Sr have less distorted structures.

B. Fe *K*-edge extended x-ray absorption fine structure spectroscopy of $La_{1-x}Sr_xFeO_{3-\delta}$

Fe K-edge EXAFS spectra were measured for the whole series $La_{1-x}Sr_xFeO_{3-\delta}$ at 35 K and at room temperature. The extracted EXAFS signals at room temperature are displayed in Fig. 3 for the sake of comparison. The spectra change continuously with increasing doping ratio as the local structure around Fe ions changes. Oscillations are still visible at $k \sim 12^{-1}$ Å, being more intense at high k for Sr-rich samples. This fact may be related to the more symmetric environment for these compounds.

The Fourier transform (FT) of the k-weighted EXAFS spectra, calculated between 2.5 and 11.5 $Å^{-1}$ using a sine window and the structural features up to 6 Å, are shown in Fig. 4. The FT spectra exhibit a continuous evolution with the doping ratio as well. The spectrum of $LaFeO_3$ shows a strong peak at ~1.55 Å corresponding to the Fe-O distance

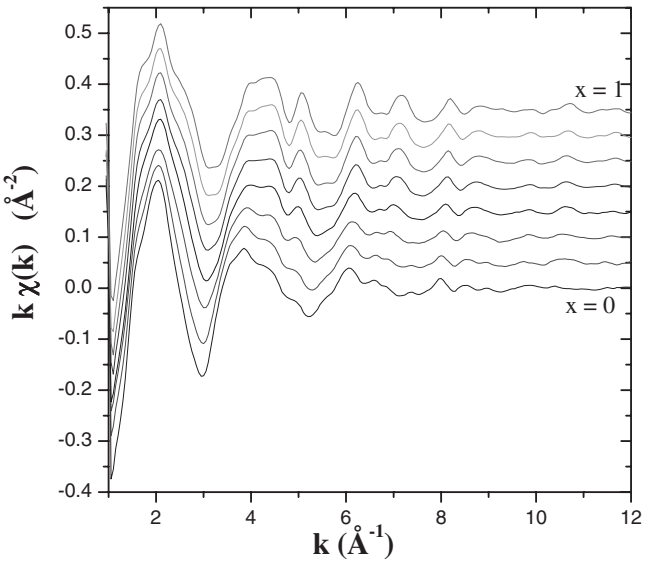

FIG. 3. EXAFS spectra, $k\chi(k)$, at the Fe K edge for the $La_{1-x}Sr_xFeO_3$ series at room temperature. The x values for each curve are (from bottom to top) 0, 1/8, 1/3, 1/2, 2/3, 3/4, 7/8, and 1. The curves are shifted upward for the sake of clarity. The background removal starts at $k=1$ $Å^{-1}$.

without a phase-shift correction. Between 2 and 3.8 Å, there are several small peaks corresponding to the second and third coordination shells, i.e., Fe-La and Fe-Fe distances. The small intensity of these peaks may be ascribed to the large number of scattering paths in the orthorhombic unit cell.

The Sr substitution for La leads to a decrease of the main peak in Fig. 4, even for small Sr doping. The intensity of this peak for samples with high Sr content remains almost constant. This could indicate a significant local disorder in the first coordination shell for the whole series except $LaFeO_3$. The position of this peak slightly shifts to lower values of R with increasing content of Sr, in agreement with the expected decrease of the Fe-O bond length. The changes observed in the second and third shells are stronger. The Sr doping leads to an increase of intensity of the corresponding peaks in the FT spectra. This can be attributed to the symmetry increase of the unit cell from orthorhombic to cubic along the whole series. In the cubic environment, the number of different Fe-Sr(La) paths around the Fe atom is strongly reduced.

The structural analysis was carried out between 1 and 4 Å in the R space fitting mode using the ARTEMIS software.[25] We have considered contributions from single scattering paths, Fe-O, Fe-Fe, and Fe-Sr(La), together with multiple scattering paths, mainly Fe-O-O and Fe-O-Fe. The best fits are also plotted in Fig. 4 as continuous lines, whereas refined distances, Debye-Waller (DW) factors, and reliability factors are summarized in Table II. In these fits, the coordination numbers were fixed to their crystallographic values, and the amplitude reduction factor s_0^2 was set at 0.69, following previous calculations.[29,30] Therefore, only bond lengths, DW factors, and threshold energy (E_0) were refined. Overall, the EXAFS results concur with the crystallographic data (compare Fe-O distances between Tables I and II). We noticed that the Fe-O bond length decreases with increasing x and,

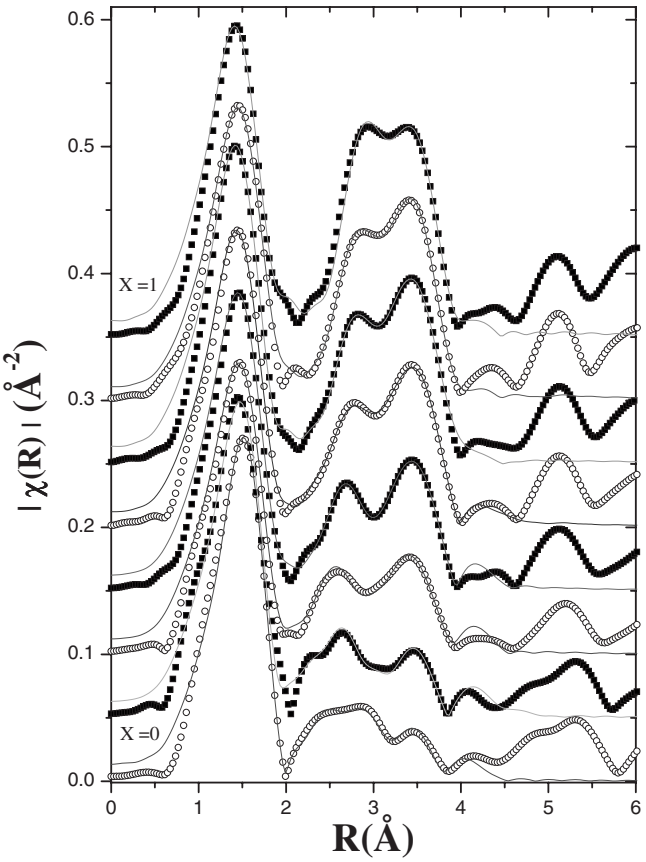

FIG. 4. Modulus of the Fourier transforms extracted from the curves of Fig. 3 using a sine window between 2.5 and 11.5 $Å^{-1}$. Solid lines are the best-fit simulations only considering contributions between 1 and 4 Å. The x values are (from bottom to top) 0, 1/8, 1/3, 1/2, 2/3, 3/4, 7/8, and 1. The curves are shifted upward for the sake of clarity.

accordingly, the oxidation state of Fe atoms increases, in agreement with the XANES spectroscopy. However, large DW factors for Fe-O distances are observed for all samples except $LaFeO_3$. DW factors are already large for the minimum doping ratio, confirming that small La substitution leads to a local disorder in the first coordination shell. Moreover, it is noteworthy that this local disorder is the highest for intermediate compositions $1/3 \leqslant x \leqslant 3/4$, including the region where the MI transition occurs.

C. Phase transition for $2/3 \leqslant x \leqslant 3/4$

In order to characterize possible structural and electronic changes across the so-called CO transition, we studied the temperature dependence of both crystal and local structures. Figure 5(a) shows the temperature evolution of the lattice parameters for $La_{1/3}Sr_{2/3}FeO_3$ down to 77 K. This composition crystallizes in a rhombohedral R-3c cell, which has been refined using the hexagonal setting. As it was found in previous studies,[9,11] the absence of superstructure reflections at low temperatures allow us to refine all XRD patterns in the same space group. The temperature variations of the lattice parameters show the usual contraction on cooling, but with anomalies in the vicinity of the phase transition. These anomalies are more pronounced for the a parameter, which shows a dip around 200 K [see Fig. 5(a)]. The curve for the c parameter shows a slope change with a small plateau at the same temperature. The large variation of parameter a may be related to the fact that the easy axis of magnetization lies in the xy plane[11] and the phase transition is accompanied by a long-range antiferromagnetic ordering (see Fig. 1).

The structural changes at the phase transition are quite smooth for the $La_{1/4}Sr_{3/4}FeO_3$ sample. We compare the temperature evolution of the unit cell volume of both samples in Fig. 5(b). A change in the slope is hardly noticeable for the $x=3/4$ compound. Such behavior may be related to several facts. First of all, the metal-insulator and magnetic transitions are not coupled for this sample (see Fig. 1). Second, the doping ratio may not be optimal for the electronic localization, and, finally, the high crystal symmetry, which is cubic in this case, may obscure slight structural changes.

In order to gain insight into the changes of the local structure around Fe atoms in both samples, we have measured EXAFS and XANES spectra between 295 and 35 K. We

TABLE II. Best fit parameters [average bond lengths, Debye-Waller, threshold energy, and reliability (Refs. 24 and 25) factors] obtained from the fitting of the EXAFS data in the R-space mode. Numbers in parentheses refer to standard deviations of the last significant digits. In the case of several distances, we report the average value, and the standard deviation corresponds to coupled displacements in order to preserve the crystal structure. The s_0^2 factor was fixed to 0.69 (Refs. 29 and 30), and the crystallographic values were taken as coordination numbers.

Sample (x)	0	1/8	1/3	1/2	2/3	3/4	7/8	1
⟨Fe-O⟩ (Å)	2.004(9)	1.994(9)	1.961(8)	1.954(8)	1.927(8)	1.920(8)	1.915(7)	1.909(8)
σ^2 (Å^2)$\times 10^{-3}$	2.5(6)	4.3(9)	6.2(12)	6.3(14)	5.5(14)	5.1(13)	4.1(12)	4.4(13)
⟨Fe-Sr⟩ (Å)	3.410(39)	3.360(35)	3.354(31)	3.353(21)	3.341(18)	3.346(12)	3.341(10)	3.332(11)
σ^2 (Å^2)$\times 10^{-3}$	7.2(13)	7.2(15)	4.8(11)	4.5(10)	7.1(13)	5.6(11)	4.6(10)	6.5(14)
⟨Fe-Fe⟩ (Å)	3.972(84)	4.002(87)	3.951(75)	3.904(46)	3.872(33)	3.856(14)	3.858(9)	3.841(10)
σ^2 (Å^2)$\times 10^{-3}$	10.5(16)	10.5(15)	10.6(16)	9.2(13)	7.5(12)	6.8(12)	6.6(12)	6.6(11)
E_0 (eV)	−2.1(6)	−1.8(6)	−2.4(8)	−1.9(5)	−2.6(6)	−4.1(7)	−4.0(8)	−3.8(7)
R-Factor	0.013	0.015	0.019	0.010	0.009	0.012	0.018	0.007

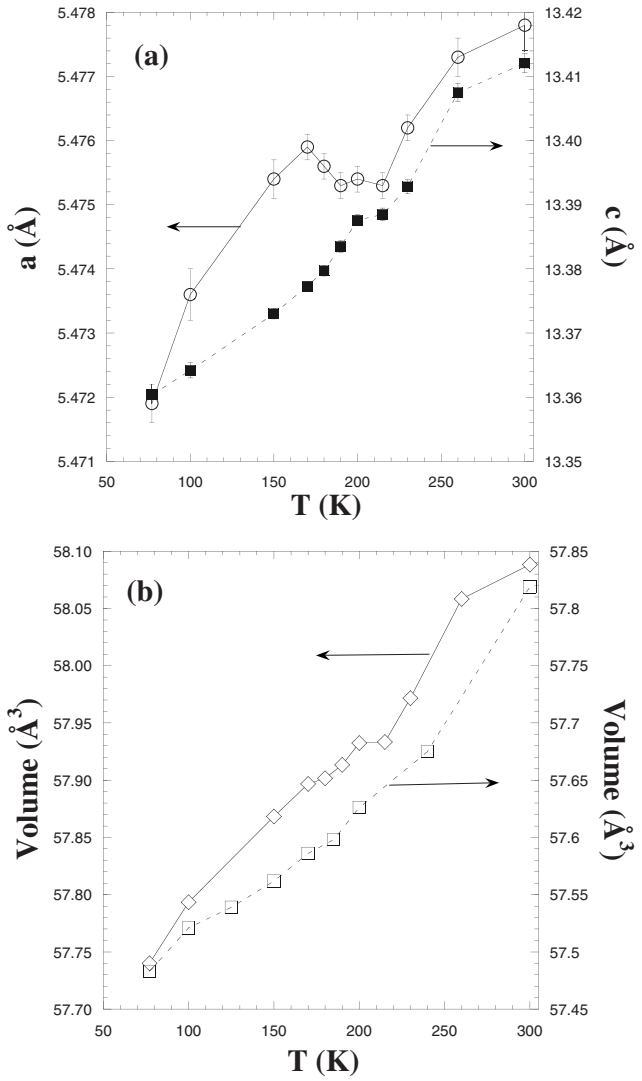

FIG. 5. (a) Temperature evolution of lattice parameters for $La_{1/3}Sr_{2/3}FeO_3$. (b) Unit cell volume/f.u. vs temperature for $La_{1/3}Sr_{2/3}FeO_3$ (diamonds) and $La_{1/4}Sr_{3/4}FeO_3$ (squares).

have also measured these spectra for $SrFeO_{2.96}$, a material without CO transition, in order to have a reference. The XANES spectra are alike in the whole temperature range for all of the three samples. The lack of noticeable changes in the energy line shape or chemical shifts indicates that only tiny changes in the electronic and/or geometrical structure can occur at the Fe atoms across the transition. This also concurs with the slight changes observed in the x-ray patterns.

The EXAFS analysis allowed us to obtain more detailed information on the local structure around the Fe atoms. Figure 6 shows the temperature dependence of Fe-O bond lengths for $La_{1/3}Sr_{2/3}FeO_3$, $La_{1/4}Sr_{3/4}FeO_3$, and $SrFeO_{2.96}$. Overall, these distances slightly decrease with decreasing temperature. However, the temperature evolution seems to be different for $SrFeO_{2.96}$ with respect to the other two samples. The former shows a continuous decrease on cooling, whereas $La_{1/3}Sr_{2/3}FeO_3$ and $La_{1/4}Sr_{3/4}FeO_3$ exhibit a small jump around 200 K near T_N (see Fig. 1) and an anomaly in the

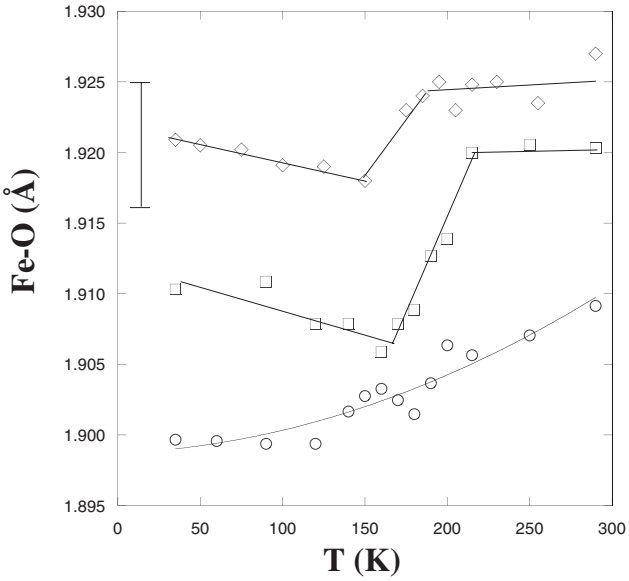

FIG. 6. Temperature evolution of the Fe-O bond length for $La_{1/3}Sr_{2/3}FeO_3$ (diamonds), $La_{1/4}Sr_{3/4}FeO_3$ (squares), and $SrFeO_3$ (circles). Lines are guides for the eyes. The typical error bar is also shown for the sake of comparison.

lattice parameters (Fig. 5). These data seem to point out to a significant role of the first coordination shell of O atoms in the above properties. To gain more insight, we have also studied the temperature evolution of the DW factors of the first, second, and third shells for these three samples. The results are depicted in Fig. 7. The expected trend for the DW factors is to decrease upon cooling as thermal vibrations decrease. Indeed, we observe such behavior in the Fe-Sr(La) paths (second shell) in all of the three samples. However, the DW factors for the first shell are anomalously large for $La_{1/3}Sr_{2/3}FeO_3$ and $La_{1/4}Sr_{3/4}FeO_3$ samples even at low temperature (below the MI transition). In addition, they show a minimum around 180 K. For $SrFeO_{2.96}$, the DW factor decreases down to 100 K, and then it slightly increases upon cooling. This temperature corresponds to the electronic localization observed in $SrFeO_{2.96}$.[13] Finally, the third shell displays an intermediate behavior between both previous shells. Here, the different behavior at low temperature for $SrFeO_{2.96}$ on the one side and for the $La_{1/3}Sr_{2/3}FeO_3$ and $La_{1/4}Sr_{3/4}FeO_3$ on the other side is more evident. The $x=2/3$ and $\frac{3}{4}$ samples show an additional disorder at low temperature, which mainly affects the Fe-O-Fe sublattice.

IV. DISCUSSION

Our results clearly show a continuous change in the structural and electronic properties of Fe atom along the series $La_{1-x}Sr_xFeO_{3-\delta}$, which we discuss below. XANES spectra reveal a chemical shift toward higher energies with increasing doping ratio. This trend is usually ascribed to an oxidation from Fe^{3+} ($LaFeO_3$) to Fe^{4+} ($SrFeO_3$).

In order to check if doped samples could be formed by a mixture of formal Fe^{3+} and Fe^{4+}, we have taken experimental XANES spectra for $LaFeO_3$ and $SrFeO_3$ as references for

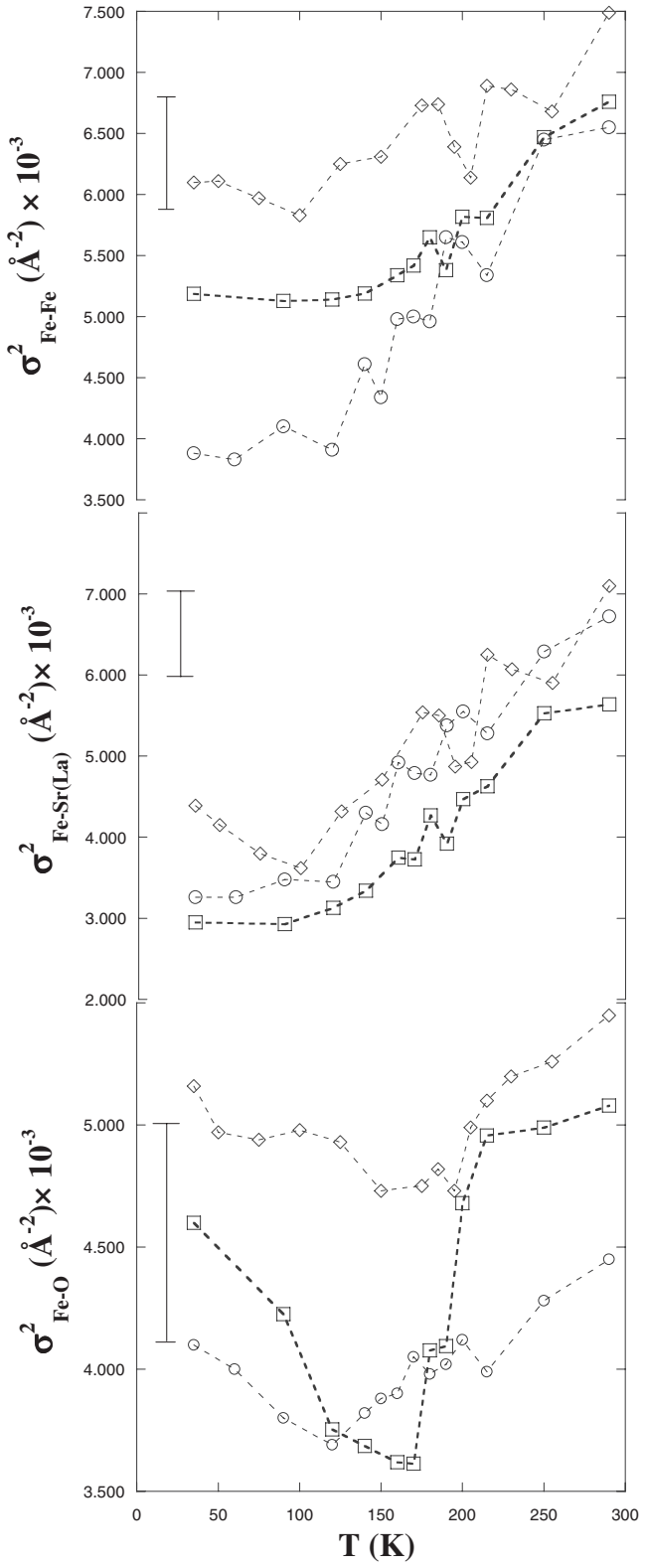

FIG. 7. Temperature evolution of DW factors for $La_{1/3}Sr_{2/3}FeO_3$ (diamonds), $La_{1/4}Sr_{3/4}FeO_3$ (squares), and $SrFeO_3$ (circles). From bottom to top: The Fe-O, Fe-Sr(La), and Fe-Fe shells. The typical error bar is also shown for the sake of comparison.

formal 3+ and 4+ oxidation states, respectively. Then, we have tested if a linear combination of both reference spectra based on the Sr content can reproduce the features of intermediate compositions. This procedure was used in the past to demonstrate that doped manganites were composed of intermediate mixed valence $Mn^{3.\delta+}$ ions instead of a mixture of Mn^{3+} and Mn^{4+} ions.[31]

The results for $x=2/3$ at two temperatures is displayed in Fig. 8. The plots show that the weighted addition (or simulated spectrum) nicely reproduces the energy position of the spectrum for $La_{1/3}Sr_{2/3}FeO_3$. The simulation also reproduces the line shape of the edge including the pre-edge features. Similar results were found for the rest of the series. Therefore, a mixture of $(1-x)$ Fe^{3+} and (x) Fe^{4+} ions can account for the XANES spectra of doped samples. Nevertheless, an intermediate valence state cannot be excluded.

The most striking point of this analysis is that the linear interpolation between the two end members also works for the $La_{1/3}Sr_{2/3}FeO_3$ XANES below the so-called CO transition temperature, as shown in Fig. 8(b). Bearing in mind that a charge disproportionation of $2Fe^{4+}$ into Fe^{3+} and Fe^{5+} implies an increase of Fe^{3+}, one would expect that a $La_{1/3}Sr_{2/3}FeO_3$ XANES spectrum would be better reproduced by a linear combination of 67% $LaFeO_3$ XANES +33% $SrFeO_3$ XANES spectra (assuming no large differences between Fe^{4+} and Fe^{5+}) instead of the reverse proportion (33% $LaFeO_3$+67% $SrFeO_3$). We have positively verified that the first assumption is worse than the second one, as shown in Fig. 8. This result, in addition to the lack of significant changes in the XANES spectra across the CO transition, is difficult to compromise with a full charge disproportionation $(2Fe^{3+}+1Fe^{5+})$ in $La_{1/3}Sr_{2/3}FeO_3$ at low temperature.

EXAFS and XRD refinements show that Fe-O distances also decrease as the doping ratio increases. This agrees with the increase of the formal oxidation state of Fe ions. However, the EXAFS analysis also reveals that the lowest DW factor of the first coordination shell corresponds to the $LaFeO_3$, even at room temperature. It seems that Sr doping leads to an increase of disorder in this coordination shell, although the crystallographic structure becomes more symmetrical with the increase of Sr content. Moreover, this disorder is stronger at intermediate compositions, close to the stoichiometry exhibiting the MI transition at low temperature $(x\sim 2/3)$, as can be seen in Table II.

A structural origin for the so-called CO transition is clear from the changes observed in the lattice parameters. However, these changes are so small that it is very hard to detect any change in the crystal symmetry. The EXAFS analysis of samples showing this transition gives us more information about its nature. The FT spectra in Fig. 4 have been fitted using the crystallographic information from Table I; for instance, in the case of $La_{1/3}Sr_{2/3}FeO_3$, the Fe is sixfold coordinated to oxygen atoms at only one distance. Fe-O shows slight changes upon cooling with a dip at the phase transition temperature, but the DW factor associated with this path is very large in the low-temperature phase. All of this points out to an increase of disorder opposite to the diminution of thermal vibrations. However, this disorder only seems to affect the Fe-O-Fe sublattice since the DW factor for the sec-

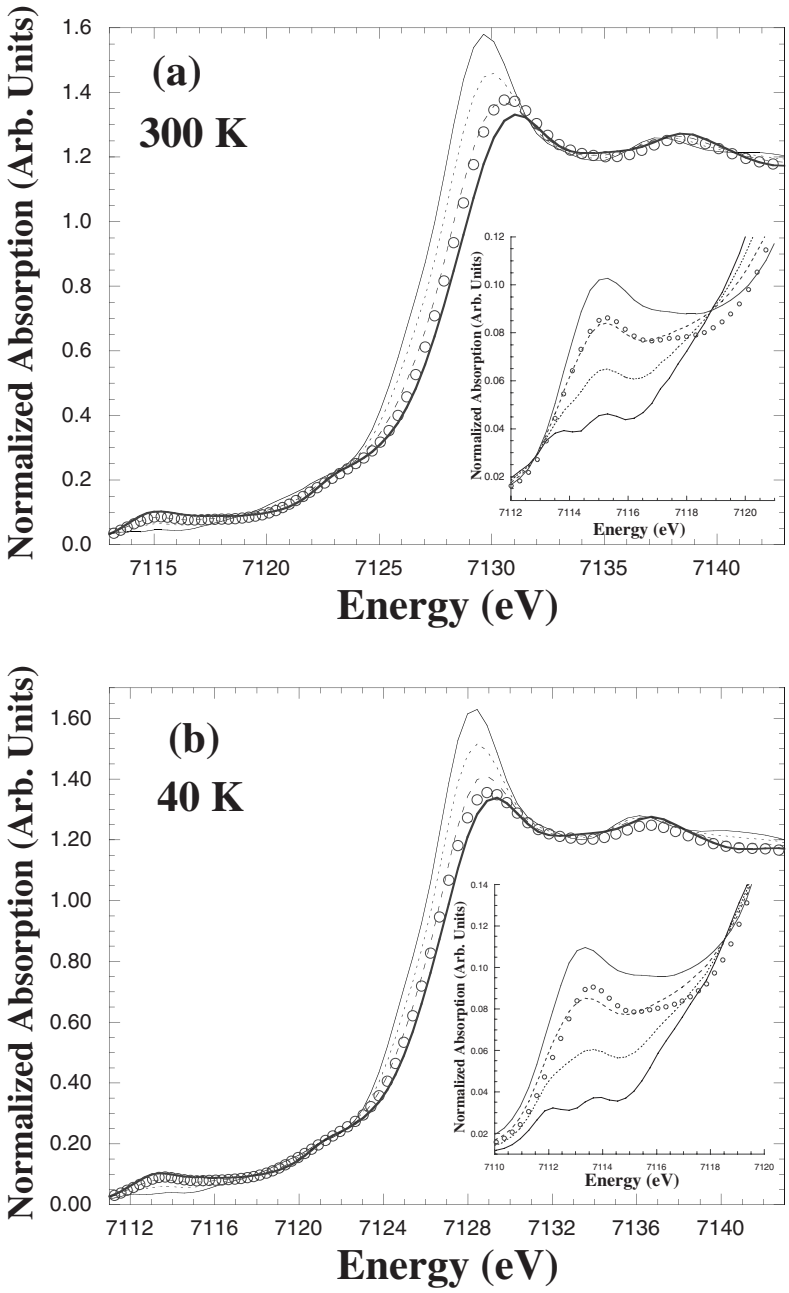

FIG. 8. Comparison between the normalized XANES spectra of $La_{1/3}Sr_{2/3}FeO_3$ (circles) and the following additions of reference XANES: $1/3LaFeO_3+2/3SrFeO_3$ (dashed line) and $2/3LaFeO_3+1/3SrFeO_3$ (dotted line). Panels (a) and (b) refer to data at 300 and 40 K, respectively. Normalized XANES spectra of parent compounds $LaFeO_3$ (thin solid line) and $SrFeO_3$ (thick solid line) are also plotted for the sake of comparison.

ond shell behaves as expected (see Fig. 7). If a charge disproportionation occurs at the phase transition, inducing more disorder in the electronic configuration of the Fe atom, one would expect related changes in all coordination shells. Since the Fe-O-Fe sublattice is the most affected, it is likely that oxygen atoms surrounding Fe ions play an important role in the localization of holes.

To gain more quantitative insight into these local structural changes, the following analysis has been carried out: Following XANES results, the $La_{1/3}Sr_{2/3}FeO_3$ sample can be considered as composed of 1/3 of Fe^{3+} and 2/3 of Fe^{4+} ions. In this case, an equivalent local structure would be composed of $1/3Fe^{3+}$-O (long) and $2/3Fe^{4+}$-O (short) distances. We have used 2.0 and 1.91 Å as Fe^{3+}-O and Fe^{4+}-O distances, respectively, i.e., experimental values obtained for $LaFeO_3$ and $SrFeO_3$ (see Table II). We were successful in fitting the experimental EXAFS spectra of $La_{1/3}Sr_{2/3}FeO_3$ at room temperature using this pair of distances. Figure 9 shows the Fourier filtered EXAFS spectra arising from atoms in the first coordination shell (1.1 Å $\leqslant R \leqslant$ 1.8 Å). We also report the best fits using a single distance (see Table II) and the above mentioned two distances. Both models show similar goodness of the fit, and the EXAFS analysis is not sensitive to the difference between a mixed valence ($Fe^{3.67+}$) and an Fe^{3+}/Fe^{4+} mixture, as we found also in the XANES spectra analysis. However, the most striking point is that these models also work for the EXAFS spectra of the same sample at 40 K where the charge disproportionation is thought to be established [see Fig. 9(c)].

A full disproportionation implies that two Fe^{4+} ions transform into Fe^{3+} and Fe^{5+} ions, leading to the change of two short Fe^{4+}-O distances into one large Fe^{3+}-O and another

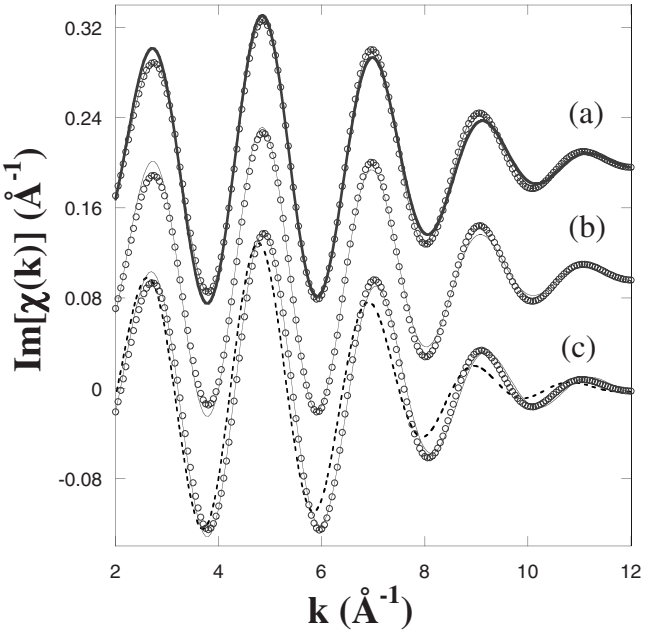

FIG. 9. Fourier filtered EXAFS spectra (circles) of the first coordination sphere around Fe atoms in $La_{1/3}Sr_{2/3}FeO_3$ at 290 [(a) and (b)] and at 40 K (c). The lines correspond to the best fits using: (a) a first coordination shell composed of $6Fe^{3.67+}$-O distances, (b) a first coordination shell composed of $2Fe^{3+}$-O and $4Fe^{4+}$-O distances, and (c) a first coordination shell composed of $2Fe^{3+}$-O and $4Fe^{4+}$-O (solid line) compared to that composed of $4Fe^{3+}$-O and $2Fe^{5+}$-O distances (dotted line).

very short Fe^{5+}-O distance. We have taken as an Fe^{5+}-O distance the value reported for $CaFeO_3$, i.e., 1.86 Å.[32] Then, we have tried to fit the EXAFS spectra using a first coordination shell composed of $2/3Fe^{3+}$-O (long) and $1/3Fe^{5+}$-O (short). The result of this fit is also displayed in Fig. 9. This fit is much worse than the previous one, and there is a phase shift between the Fe^{3+}-Fe^{5+} model and the experimental oscillations, very evident at high k. The use of higher values for Fe^{5+}-O distances (up to 1.91 Å) or lower values for Fe^{3+}-O bonds (down to 1.97 Å) does not improve it significantly. This indicates that the phase shift is not only related to the average distance but also to the ratio of scattering centers so that the experimental oscillation can only be reproduced either by only one distance with a large Debye-Waller factor or by the addition of 2/3 short and 1/3 long Fe-O distances. This result strongly disagrees with the presence of a significant charge disproportionation in this sample, implying the presence of $2/3Fe^{3+}$ (big) and $1/3Fe^{5+}$ (small) cations.

A first sight could suggest that our results are at odds with previous neutron studies, but a detailed inspection reveals that both kinds of studies could concur in the same point. The magnetic structure was refined using a sequence 533533 along the z axis in the frame of the hexagonal setting of the R-3c space group.[8] The authors assumed antiferromagnetic Fe^{3+}-O-Fe^{3+} and ferromagnetic Fe^{3+}-O-Fe^{5+} interactions lying in the magnetic moments along the xy plane. Structural constrains were needed to stabilize the refinement, and the magnetic moments were refined to $3.61\mu_B$ and $2.76\mu_B$ for Fe^{3+} and Fe^{5+} sites, respectively.[8] Other authors obtained significant smaller values for the magnetic moments, evidencing the difficulty of this refinement.[11]

Battle *et al.*[8] were surprised by the absence of any significant structural distortion accompanying the 2:1 ordering of Fe^{3+} and Fe^{5+}, and they deduced the existence of nonintegral charge states in agreement with Takano *et al.*[6] Battle *et al.* literally stated that assuming a linear correlation of electron charge and flux density between $Sr_2Fe_2O_5$ and $SrFeO_3$, the Fe^{3+} site in $La_{1/3}Sr_{2/3}FeO_3$ has an actual charge of approximately +3.4, and hence the actual charge of the Fe^{5+} site is only approximately +4.2. This conclusion is in agreement with our experimental results, which makes evident the absence of Fe^{+5} in this system. Furthermore, if we considered that disproportionation only concerns Fe^{4+}, $2Fe^{4+} \rightarrow Fe^{4+\delta} + Fe^{4-\delta}$, δ would have a value around 0.2 and the "Fe^{3+} site" would be formed by a mixture of Fe^{3+} and $Fe^{3.8+}$ (average of +3.4). The point emphasized by our experiments is that this kind of disproportionation, if it exists, should be very small ($\delta \rightarrow 0$).

Concerning the metal-insulator transition, one must take into account the presence of a significant disorder at room temperature in doped samples. We think that a structural transition from uncorrelated different FeO_6 octahedra at room temperature to a low-temperature phase with an ordering of these octahedra might be a suitable explanation for the metal-insulator phase transition observed in the $La_{1/3}Sr_{2/3}FeO_3$ and $La_{1/4}Sr_{3/4}FeO_3$. Distortions are dynamic in the high-temperature phase and static at low temperature. Its localization could drive to a lattice symmetry change, giving rise to new cell where different iron sites exist.[10,11] Such sites should be identified as Fe^{3+} and Fe^{4+} and not as Fe^{3+} and Fe^{5+}. In this sense, the phase transition can be described as an order-disorder phase transition between dynamic and static distortions.

V. CONCLUSIONS

The crystal and local structures have been studied for $La_{1-x}Sr_xFeO_{3-\delta}$ samples. Diffraction and spectroscopic results show a continuous change of Fe valence as La is substituted with Sr. This result is clearly seen in a chemical shift of 1.26 ± 0.2 eV of the Fe K-edge XANES spectra and a continuous diminution of Fe-O distances as x increases.

XANES and EXAFS spectroscopies reveal that hole doping produces disorder in the local structure around the Fe ions in these samples, even at temperatures above the MI transition. This disorder gives rise to the large DW factor values observed for the Fe-O distances. The largest DW factors are found for compositions close to the ones where the MI transition takes place at low temperature. Moreover, the DW factors related to the Fe-O-Fe sublattice (Fe-O or Fe-Fe) increase or remain quite large below the MI transition upon cooling. However, the DW factor of the second coordination shell (Fe-Sr) follows the usual thermal trend, suggesting an important role of oxygen atoms in the local disorder.

So far, we cannot determine what kind of mixed valence exists along the whole series $La_{1-x}Sr_xFeO_3$, i.e., if it is pure intermediate valence $Fe^{3.x+}$ or a mixture of Fe^{3+} and Fe^{4+}. We can reproduce the XANES spectra of the series members by

the weighted addition of XANES spectra from Fe^{3+} and Fe^{4+} of the parent compounds. This is true even at low temperatures where it is thought that the Fe^{4+} disproportionates into Fe^{3+} and Fe^{5+} for $x \sim 2/3$. Moreover, the ratio $2Fe^{3+} + 1Fe^{5+}$ cannot account for both XANES and EXAFS spectra of $La_{1/3}Sr_{2/3}FeO_3$ below the phase transition temperature. This result points to the lack of significant charge disproportionation in this system. Therefore, the metal-insulator transition is likely to be an order-disorder transition. Distortions are dynamic at high temperature, allowing electronic conduction, but they are freezing below the phase transition temperature. This localization leads to an ordered arrangement of two different FeO_6 octahedra, giving rise to slight structural changes able to show superstructure peaks in some cases.[9–11]

ACKNOWLEDGMENTS

The authors acknowledge the financial support from CICyT (Project No. MAT05-04562) and DGA (CAMRADS and PIP018/2005). They thank ESRF for granting beam time and the BM29 team for help during the experiment.

*Corresponding author; jbc@unizar.es

[1] T. Ishikawa, S. K. Park, T. Katsufuji, T. Arima, and Y. Tokura, Phys. Rev. B **58**, R13326 (1998).
[2] G. Chern, W. K. Hsieh, M. F. Tai, and K. S. Hsung, Phys. Rev. B **58**, 1252 (1998).
[3] L. White, J. Appl. Phys. **40**, 1061 (1969).
[4] A. Wattiaux, J. C. Grenier, M. Pouchard, and P. Hagenmuller, J. Electrochem. Soc. **134**, 1718 (1987).
[5] J. B. MacChesney, R. C. Sherwood, and J. F. Potter, J. Chem. Phys. **43**, 1907 (1965).
[6] M. Takano, J. Kawachi, N. Nakanishi, and Y. Takeda, J. Solid State Chem. **39**, 75 (1981).
[7] J. Matsuno, T. Mizokawa, A. Fujimori, Y. Takeda, S. Kawasaki, and M. Takano, Phys. Rev. B **66**, 193103 (2002).
[8] P. D. Battle, T. C. Gibb, and P. Lightfoot, J. Solid State Chem. **84**, 271 (1990).
[9] J. Q. Li, Y. Matsui, S. K. Park, and Y. Tokura, Phys. Rev. Lett. **79**, 297 (1997).
[10] R. Kajimoto, Y. Oohara, M. Kubota, H. Yoshizawa, S. K. Park, Y. Taguchi, and Y. Tokura, J. Phys. Chem. Solids **62**, 321 (2001).
[11] J. B. Yang, X. D. Zhou, A. Chu, W. M. Hikal, Q. Cai, J. C. Ho, D. C. Kundaliya, W. B. Yelon, W. J. James, H. U. Anderson, H. H. Hamdeh, and S. K. Malik, J. Phys.: Condens. Matter **15**, 5093 (2003).
[12] S. K. Park, T. Ishikawa, Y. Tokura, J. Q. Li, and Y. Matsui, Phys. Rev. B **60**, 10788 (1999).
[13] J. Blasco, J. Stankiewicz, and J. García, J. Solid State Chem. **179**, 898 (2006).
[14] S. E. Dann, D. B. Currie, M. T. Weller, M. F. Thomas, and A. D. Al-Rawwas, J. Solid State Chem. **109**, 134 (1994).
[15] M. Abbate, F. M. F. de Groot, J. C. Fuggle, A. Fujimori, O. Strebel, F. Lopez, M. Domke, G. Kaindl, G. A. Sawatzky, M. Takano, Y. Takeda, H. Eisaki, and S. Uchida, Phys. Rev. B **46**, 4511 (1992).
[16] H. Wadati, D. Kobayashi, H. Kumigashira, K. Okazaki, T. Mizokawa, A. Fujimori, K. Horiba, M. Oshima, N. Hamada, M. Lippmaa, M. Kawasaki, and H. Koinuma, Phys. Rev. B **71**, 035108 (2005).
[17] A. Deb, J. M. Ralph, E. J. Cairns, and U. Bergmann, Phys. Rev. B **73**, 115114 (2006).
[18] C. L. Chang, G. Chern, M. F. Tai, Y. W. Su, C. L. Dong, S. Y. Liu, C. S. Hwang, and P. K. Tseng, Jpn. J. Appl. Phys., Part 1 **38**, 108 (1999).
[19] M. C. Sánchez, G. Subías, J. García, and J. Blasco, Phys. Rev. Lett. **90**, 045503 (2003).
[20] M. C. Sánchez, J. García, J. Blasco, G. Subías, and J. Perez-Cacho, Phys. Rev. B **65**, 144409 (2002).
[21] J. Rodríguez-Carvajal, Physica B **192**, 55 (1992).
[22] P. Karen and P. Woodward, J. Mater. Chem. **9**, 789 (1999).
[23] M. Karppinen, M. Matvejeff, K. Salomäki, and H. Yamauchi, J. Mater. Chem. **12**, 1761 (2002).
[24] A. Filipponi, M. Borowski, D. T. Bowron, S. Ansell, A. DiCicco, S. de Panfilis, and J. P. Itiè, Rev. Sci. Instrum. **71**, 2422 (2000).
[25] B. Ravel and M. Newville, J. Synchrotron Radiat. **12**, 537 (2005).
[26] J. J. Rehr and R. C. Albers, Rev. Mod. Phys. **72**, 621 (2000).
[27] R. D. Shannon, Acta Crystallogr., Sect. A: Cryst. Phys., Diffr., Theor. Gen. Crystallogr. **A32**, 751 (1976).
[28] Z. Y. Wu, D. C. Xian, T. D. Hu, Y. N. Xie, Y. Tao, C. R. Natoli, E. Paris, and A. Marcelli, Phys. Rev. B **70**, 033104 (2004).
[29] E. A. Stern, in *X-ray Absorption: Principles, Applications, Techniques of EXAFS, SEXAFS and XANES*, edited by D. C. Koninsberger and R. Prins (Wiley-Interscience, New York, 1988), p. 40.
[30] M. Roy, S. J. Gurman, and G. van Dorssen, J. Phys. IV **7**, 151 (1997).
[31] J. García, M. C. Sánchez, G. Subías, and J. Blasco, J. Phys.: Condens. Matter **13**, 3229 (2001); G. Subías, J. García, M. G. Proietti, and J. Blasco, Phys. Rev. B **56**, 8183 (1997).
[32] P. M. Woodward, D. E. Cox, E. Moshopoulou, A. W. Sleight, and S. Morimoto, Phys. Rev. B **62**, 844 (2000).